Arl4D-EB1 interaction promotes centrosomal recruitment of EB1 and microtubule growth

Shin-Jin Lin[a,b,†], Chun-Fang Huang[a,†,‡], Tsung-Sheng Wu[a], Chun-Chun Li[a,§], and Fang-Jen S. Lee[a,b,c,*]
[a]Institute of Molecular Medicine and [c]Center of Precision Medicine, College of Medicine, and [b]Department of Medical Research, National Taiwan University Hospital, National Taiwan University, 100225 Taipei, Taiwan

ABSTRACT **ADP-ribosylation factor (Arf)-like 4D (Arl4D), one of the Arf-like small GTPases, functions in the regulation of cell morphology, cell migration, and actin cytoskeleton remodeling. End-binding 1 (EB1) is a microtubule (MT) plus-end tracking protein that preferentially localizes at the tips of the plus ends of growing MTs and at the centrosome. EB1 depletion results in many centrosome-related defects. Here, we report that Arl4D promotes the recruitment of EB1 to the centrosome and regulates MT nucleation. We first showed that Arl4D interacts with EB1 in a GTP-dependent manner. This interaction is dependent on the C-terminal EB homology region of EB1 and partially dependent on an SxLP motif of Arl4D. We found that Arl4D colocalized with γ-tubulin in centrosomes and the depletion of Arl4D resulted in a centrosomal MT nucleation defect. We further demonstrated that abolishing Arl4D-EB1 interaction decreased MT nucleation rate and diminished the centrosomal recruitment of EB1 without affecting MT growth rate. In addition, Arl4D binding to EB1 increased the association between the p150 subunit of dynactin and the EB1, which is important for MT stabilization. Together, our results indicate that Arl4D modulates MT nucleation through regulation of the EB1–p150 association at the centrosome.**

Monitoring Editor
Fred Chang
University of California, San Francisco

Received: Oct 3, 2018
Revised: Jul 27, 2020
Accepted: Jul 29, 2020

This article was published online ahead of print in MBoC in Press (http://www.molbiolcell.org/cgi/doi/10.1091/mbc.E18-10-0611) on August 5, 2020.

†These authors contributed equally to this work.

Competing financial interests: The authors declare no competing financial interests.

Contributions: C.-F.H., S.-J.L., and F.-J.S.L. designed the study and interpreted the results; S.-J.L. and C.-F.H. performed the majority of the experiments and analyzed the data; T.-S.W. and C.-C.L. conducted and supported the biological experiments; C.-F.H., S.-J.L, and F.-J.S.L. wrote and edited the manuscript; F.-J.S.L. provided supervision, funding acquisition, and project administration.

Current Address: ‡National Laboratory Animal Center, National Applied Research Laboratories, 115202 Taipei, Taiwan; §Department of Life Sciences, National Cheng Kung University, 701 Tainan, Taiwan.

*Address correspondence to: Fang-Jen S. Lee (fangjen@ntu.edu.tw).

Abbreviations used: aa, amino acid; ANOVA, analysis of variance; APC, adenomatous polyposis coli; Arf, ADP-ribosylation factor; Arl, ADP-ribosylation factor-like; BD, binding domain; BSA, bovine serum albumin; CLASP, CLIP-associated protein; DSP, dithiobis (succinimidyl propionate); EBH, EB homology; EMTB, ensconsin microtubule-binding domain; FBS, fetal bovine serum; GAP, GTPase-activating protein; GEF, guanine nucleotide exchange factor; MEF, mouse embryonic fibroblast; MEM, minimum essential medium; MT, microtubule; MTOC, MT-organizing center; PBS, phosphate-buffered saline.

INTRODUCTION

ADP-ribosylation factor (Arf) and ARF-like (Arl) proteins, that is, the ARF family of small GTPases, are major regulators of membrane trafficking in exocytotic and endocytic pathways (D'Souza-Schorey and Chavrier, 2006; Donaldson and Jackson, 2011). Among them, three isoforms of Arl4 (Arl4A, Arl4C, and Arl4D) form a unique group within the family; these isoforms can be distinguished from other Arf family members by the presence of a short basic extension at the C terminus and a longer Ras-like interswitch region (Pasqualato *et al.*, 2002). The C-terminal extension of Arl4 functions as a nuclear localization signal that facilitates their interaction with importin-α and their nuclear translocation (Jacobs *et al.*, 1999; Lin *et al.*, 2000, 2002). Their Ras-like interswitch regions enable them to undergo GDP/GTP nucleotide exchange in the absence of membrane or other cellular factors (Pasqualato *et al.*, 2002; D'Souza-Schorey and Chavrier, 2006).

Studies have suggested roles for Arl4 proteins in development, differentiation, organelle morphology, and cytoskeletal dynamics (Lin *et al.*, 2000, 2002; Pasqualato *et al.*, 2002; Li *et al.*, 2007, 2012; Chiang *et al.*, 2017; Chen *et al.*, 2020). In initial studies of Arl4s, it was found that Arl4A and Arl4D mRNAs are highly expressed at embryonic day 7 but are barely detectable at day 11 (Lin *et al.*, 2000, 2002). Nucleotide-binding-defective Arl4D can localize to mitochondrial

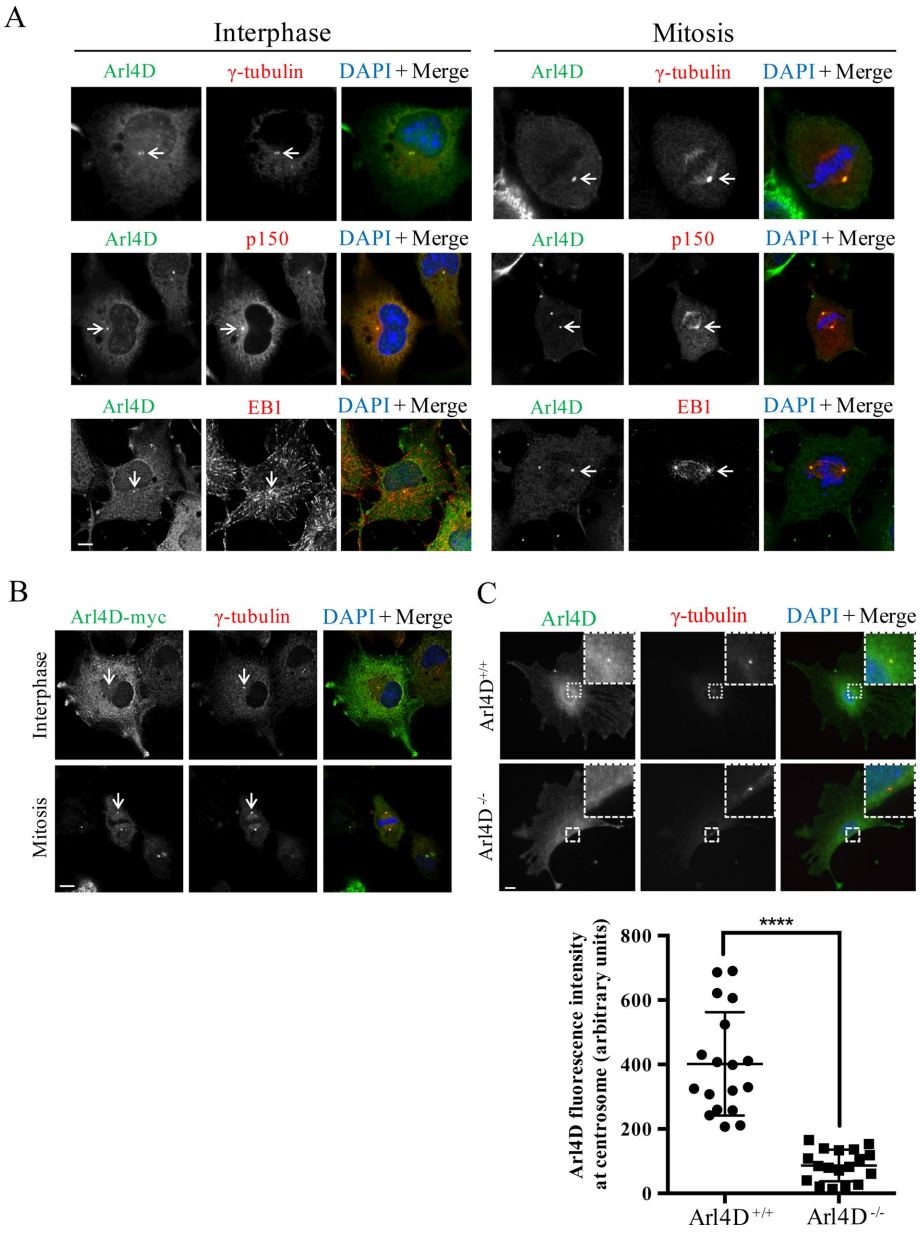

FIGURE 1: Overexpressed and endogenous Arl4D proteins localize to the centrosome. (A) COS-7 cells were transfected with untagged Arl4D and prepared for immunofluorescence staining with antibodies against Arl4D (green) together with γ-tubulin, p150, or EB1 (red). DNA were counterstained with DAPI (blue). (B) COS-7 cells transfected with Arl4D-myc were stained with antibodies against myc (green) and γ-tubulin (red). (C) Immunofluorescence labeling of Arl4D and γ-tubulin in Arl4D$^{+/+}$ and Arl4D$^{-/-}$ MEFs were analyzed by using Arl4D and γ-tubulin antibodies (top panels). Quantification of the Arl4D signals in the centrosomal region is shown in the bottom panel. The endogenous Arl4D signals in the centrosomal region of Arl4D$^{-/-}$ MEFs was significantly lower than that in Arl4D$^{+/+}$ MEFs. The solid bars in the figure indicate the mean ± SD. $N = 18$. ****$P < 0.0001$ by Student's t test. Scale bars, 10 μm.

Microtubules (MTs) are cytoskeletal components that form arrays in the cell that determine cell shape, modulate cellular motility, and support intracellular events such as intracellular transport and chromosome segregation during mitosis. MT arrays are nucleated from the MT-organizing center (MTOC), which is usually coupled to the centrosome or to cellular organelles such as the Golgi apparatus, melanosomes, or the nuclear envelope (Barral and Seabra, 2004; Wu and Akhmanova, 2017). MT nucleation and anchoring activities at the centrosome are regulated by multiple protein complexes, but the processes involved have not been fully elucidated. One of the complexes that is important for MT nucleation and anchoring at the centrosome is the dynactin complex (Delgehyr *et al.*, 2005; Hayashi *et al.*, 2005; Strickland *et al.*, 2005). Interaction between p150, a component of the dynactin complex, and end-binding 1 (EB1), an MT plus-end tracking protein, has been shown to be necessary for the assembly of a radial MT array during the formation of the centrosome (Askham *et al.*, 2002; Louie *et al.*, 2004; Vaughan, 2005). EB1 is a member of the EB family, which consists of three different members: EB1, EB2 (RP1), and EB3 (EBF3) (Su *et al.*, 1995; Renner *et al.*, 1997; Juwana *et al.*, 1999; Nakagawa *et al.*, 2000; Su and Qi, 2001). EB proteins regulate MT dynamics and participate in the organization of MTs within the cell (Vaughan, 2005; Coquelle *et al.*, 2009). Depletion of EB1 results in many centrosome-related defects, including defects in MT organization, cell motility, and primary cilia formation (Wen *et al.*, 2004; Schrøder *et al.*, 2007).

In this study, we observed that Arl4D and EB1 both localize to the centrosome, and that Arl4D interacts with EB1 in a GTP-dependent manner. We further demonstrated that the Arl4D-EB1 interaction is important for EB1 recruitment to the centrosome and that it regulates MT nucleation from the centrosome. Finally, we showed that Arl4D may stabilize the association between the p150 subunit of dynactin and EB1. Thus, we propose that Arl4D binding to EB1 regulates MT nucleation at the centrosome via modulation of the EB1–p150 association.

inner membranes, and its expression alters mitochondrial morphology and membrane potential (Li *et al.*, 2012). Overexpression of activated Arl4D can recruit cytohesin-2/ARNO, the guanine nucleotide exchange factor (GEF) for Arf6, to the plasma membrane to promote Arf6 activation, leading to modulation of actin dynamics and affecting cellular processes such as cell migration and neurite outgrowth (Li *et al.*, 2007; Yamauchi *et al.*, 2009). Although previous studies have reported the putative roles of Arl4s, a complete picture of the regulation of their function has not emerged.

RESULTS

Arl4D localizes to the centrosome

We reported previously that Arl4D could localize to the plasma membrane, mitochondria, nucleus, and perinuclear region (Li *et al.*, 2007, 2012). Furthermore, we often observed Arl4D distributed throughout the cytoplasm, with signal of dense spot(s) localized in the perinuclear region during interphase and mitosis in untagged Arl4D-overexpressed COS-7 cells immunostained with specific antibody against Arl4D (Figure 1 and Supplemental Figure S1A). This

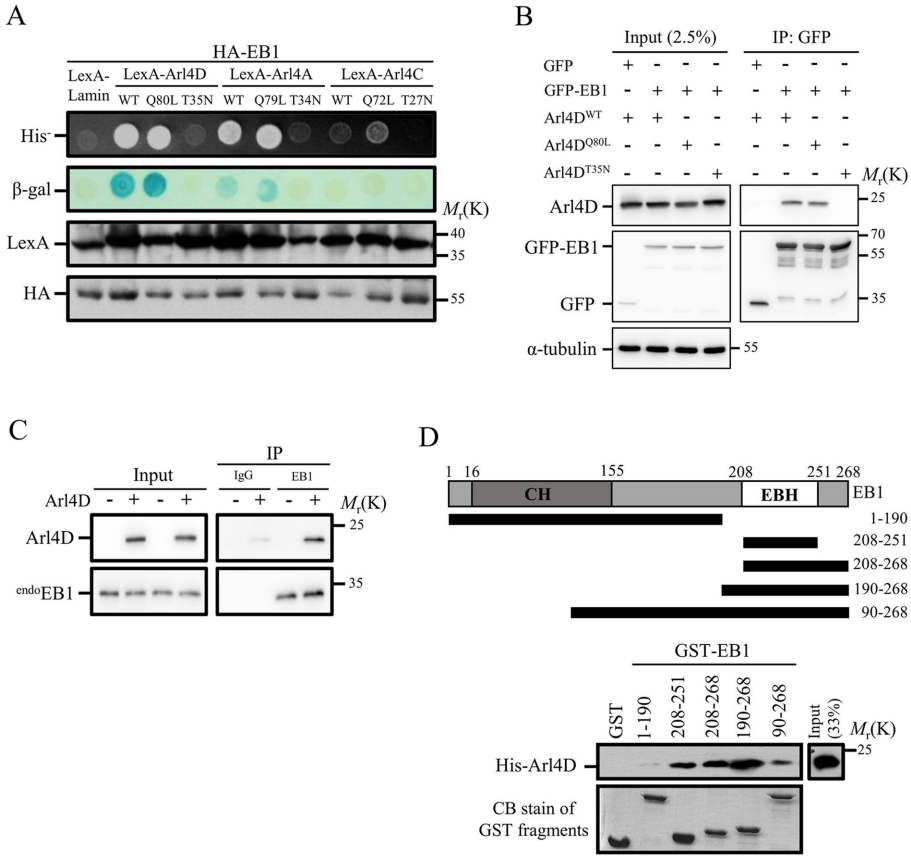

FIGURE 2: Arl4D interacts with EB1 in a nucleotide-dependent manner. (A) Arl4D and Arl4A, whether in their WT or constitutively active forms, interact with EB1 in the yeast two-hybrid system. L40 yeast cultures cotransformed with Gal4p-activation domain fusions of HA-EB1 and LexA-DNA-BD fusions of the indicated Arl4 proteins were analyzed for their β-galactosidase activity and for growth on selective medium lacking histidine. The bottom panel shows the expression levels of the fusion proteins. (B) EB1 interacts with Arl4D^{WT} and Arl4D^{Q80L} in vivo. Lysates of COS-7 cells transfected with the indicated plasmids were immunoprecipitated with GFP-Trap beads, and the bound proteins were analyzed by Western blotting with anti-GFP, anti-Arl4D, and anti-α-tubulin antibodies. (C) Interaction of endogenous EB1 with exogenous Arl4D. Lysates of COS-7 cells with or without exogenously expressed Arl4D were immunoprecipitated with EB1 antibodies, and the bound proteins were analyzed by Western blotting with antibodies against Arl4D and EB1. Mouse IgG was used as a negative control. (D) The EB1 EBH domain is sufficient to mediate EB1–Arl4D interaction. The interaction of Arl4D with different fragments of EB1 was assessed by in vitro GST pull-down assays. The top panel shows a schematic illustration of the domain organization of EB1 protein and the fragments used in this study, including calponin homology domains (aa 16–155) and the EBH domain (aa 208–251). Purified His-tagged Arl4D was incubated either with GST or with the indicated GST-EB1 fragments immobilized on glutathione Sepharose 4B beads. The proteins pulled down by the glutathione Sepharose 4B beads were analyzed by Western blotting with anti-His antibodies. The amount of GST and GST-fusion proteins in each assay was assessed by Coomassie Blue staining.

signal colocalized with γ-tubulin, p150, and EB1 signals, indicating possible centrosomal localization (Figure 1A). In addition, we did not observe Arl4D colocalized with EB1 at MT plus ends. Colocalization of endogenous and exogenous Arl4D with γ-tubulin was also observed in mitotic COS-7 and HeLa cells (Supplemental Figure S1B). This centrosome-localized signal was diminished when we preincubated the antibody with an Arl4D epitope-specific peptide (Supplemental Figure S1C). To eliminate the nonspecific signal produced by polyclonal antibodies, the localization of C-terminal myc-tagged Arl4D was examined. The distribution of Arl4D-myc was similar to that of untagged Arl4D: Arl4D-myc was localized around the centrosome during mitosis and interphase (Figure 1B). To rule out the possibility that the centrosomal signal was due to nonspecific staining of the myc antibody, we stained untransfected cells with anti-myc antibody. Under extended exposure, the antibody did not show a centrosomal signal, although some diffuse signal distributed throughout the cell was observed under oversaturating imaging conditions (Supplemental Figure S2). In mouse embryonic fibroblasts (MEFs) from Arl4D$^{+/+}$ mice, anti-Arl4D antibody also labeled the centrosomal structure. MEFs from Arl4D$^{-/-}$ animals showed less prominent centrosomal labeling than those from Arl4D$^{+/+}$ animals (Figure 1C). To examine whether the localization of Arl4D to the centrosome was GTP-dependent, we expressed Arl4D^{WT}, constitutively active (Arl4D^{Q80L}), and GTP-binding-defective (Arl4D^{T35N}) Arl4D protein at low levels in COS-7 cells. We found that signals from Arl4D^{WT} and Arl4D^{Q80L}, but not from Arl4D^{T35N}, could be detected at the centrosome (Supplemental Figure S1D). These results indicate that Arl4D localizes to the centrosome in a GTP-dependent manner.

EB1 is an Arl4D-interacting protein

To obtain additional clues as to the function of Arl4D at the centrosome, we screened for putative Arl4D-interacting proteins using the yeast two-hybrid assay. Arl4D^{Q80L} was used as bait to screen a mouse 7-day embryonic cDNA library. Among 61 positive clones, we identified six independent gene products. One of the Arl4D-interacting clones was identified 13 times and was found to be a C-terminal fragment of EB1 (amino acids [aa] 90–268). We subsequently cloned full-length EB1 and evaluated the Arl4-EB1 interaction using the yeast two-hybrid assay. We found that EB1 interacted with Arl4D^{WT} and Arl4A^{WT} but not with Arl4C^{WT}. In addition, EB1 interacted with both Arl4A and Arl4D in a nucleotide-dependent manner, with binding to evident WT and constitutively active forms of Arl4D and Arl4A but not to the GTP-binding-defective mutants Arl4D^{T35N} and Arl4A^{T34N} (Figure 2A).

To evaluate the interaction between Arl4D and EB1 in vivo, we performed immunoprecipitation assays. We first co-expressed N-terminally GFP-tagged, full-length EB1 protein with Arl4D^{WT}, Arl4D^{Q80L}, or Arl4D^{T35N} in COS-7 cells and subjected the cell lysates to immunoprecipitation using GFP-Trap. As shown in Figure 2B, Arl4D^{WT} and Arl4D^{Q80L}, but not Arl4D^{T35N}, co-immunoprecipitated with GFP-EB1. We failed to detect the presence of endogenous Arl4D among the proteins immunoprecipitated by antibodies against EB1 (unpublished data). Because the interaction of Arl4D with EB1 in cells may involve only very small amounts of both proteins, the insufficient sensitivity of our Arl4D-antibodies precluded

identification of endogenous Arl4D in EB1-precipitated complexes. However, by overexpressing Arl4D^{WT} and performing an immunoprecipitation assay using anti-EB1 antibodies, we were able to detect an interaction between these two proteins (Figure 2C). These results indicated that Arl4D and EB1 could interact in vivo and their interaction may be dependent on the presence of a sufficient amount of GTP-bound Arl4D. We next attempted to identify the regions of EB1 that are required for its binding to Arl4D by generating GST-tagged truncation constructs of EB1 and evaluating their ability to interact with Arl4D protein in vitro. As shown in Figure 2D, Arl4D^{WT} did not interact with the N-terminal 190 aa of EB1; however, it interacted with constructs corresponding to the C-terminal region of EB1, including those containing aa 208–251, 208–268, 190–268, and 90–268. Amino acids 208–251 comprise the EB homology (EBH) domain of EB1, which is known to mediate the interaction of EB1 with its binding partners (Akhmanova and Steinmetz, 2010). Taken together, the evidence presented herein points to a specific interaction between Arl4D and EB1 and shows that the EBH domain of EB1 is sufficient to mediate this interaction.

Arl4D depletion resulted in diminished MT regrowth from the centrosome

EB1 is a MT plus-end binding protein that modulates MT dynamics (Askham *et al.,* 2002; Louie *et al.,* 2004). Depletion of EB1 reduces MT centrosomal anchoring and delays MT regrowth from the centrosome in MT regrowth assays (Louie *et al.,* 2004). To explore whether Arl4D, like EB1, contributes to MT regrowth from the centrosome, we examined centrosomal MT regrowth under Arl4D-depleted conditions. We used pSuper-shRNA plasmids with sequences targeting Arl4D to knock down Arl4D expression in COS-7 cells. Cellular MTs were depolymerized with nocodazole and cold treatment as described in *Materials and Methods*. MT regrowth was monitored after nocodazole washout with warm medium. In three independent experiments, we found that the majority (62–72.5%) of the control shRNA-treated cells showed well-focused, prominent MT asters 30 s after nocodazole washout. Consistent with previous reports (Louie *et al.,* 2004), MT regrowth and aster formation from the centrosome were disrupted by EB1 depletion, with only 22.5–34% of the cells showing MT asters (Figure 3, A and B, EB1 shRNA-treated cells). In Arl4D-depleted cells, we observed prominent MT asters in only 30–33.4% of cells. The percentage of cells with MT asters was significantly lower than the percentage of control cells with asters ($p < 0.001$, Figure 3, A and B). Decrease in EB1 or Arl4D protein levels after shRNA knockdown is shown in Figure 3C. To further characterize the MT regrowth defect in Arl4D-depleted cells, we expressed an mCherry-tagged ensconsin MT-binding domain (BD) (EMTB-mCherry) in siControl- and siArl4D-treated cells as a means of tracking newly nucleated MT at the centrosome after nocodazole-induced MT depolymerization and washout. Representative time-lapse images of G1/S cells are shown in Figure 3D. In siControl-treated cells, an average of 13.25 ± 2.7 MT/min (mean ± SD) were nucleated from the centrosome, while in siArl4D-treated cells, an average of 6.875 ± 3.4 MT/min (mean ± SD) were nucleated (Figure 3E). To confirm that the reduction in MT growth was Arl4D-specific, we introduced shRNA-resistant Arl4D (Arl4D^{Res}) into Arl4D-shRNA-treated cells and counted the numbers of centrosomal aster-associated MT after allowing 30 s for MT regrowth. Fixed cells were stained with antibodies against Arl4D and MTs and imaged to quantify the number of MTs. In shControl cells, the average number of MTs attached to the centrosome was 13.01 ± 3 MT/cell (mean ± SD). In Arl4D shRNA-treated cells, the number decreased to 4.34 ± 0.64 MT/cell. In Arl4D-rescued cells, 11.3 ± 2.2 MT/cell were counted. These results indicated that the effect was Arl4D specific (Figure 3F).

In MEFs from Arl4D-knockout (Arl4D$^{-/-}$) mice, we also found that the percentage of cells with well-organized, prominent MT asters was significantly lower than that in Arl4D$^{+/+}$ cells (32–41% vs. 54–77%, respectively) (Figure 4, A and B). We further quantified the number of MTs nucleated from the centrosome during regrowth in these MEF cells. Ninety seconds after nocodazole washout, there were 27.3 ± 8.4 MTs/aster (mean ± SD) in Arl4D$^{+/+}$ cells and 2.2 ± 4.1 MTs/aster (mean ± SD) in Arl4D$^{-/-}$ cells (Figure 4C). These observations indicated that the depletion of Arl4D resulted in the regrowth of fewer MTs from the centrosome after nocodazole depolymerization and washout.

We next examined the dynamics of MT growth by observing the behavior of EB1 comets. We expressed GFP-EB1 at moderate levels in siControl- and siArl4D-treated COS-7 cells and subjected the cells to time-lapse live cell imaging (Supplemental Movie S1). We analyzed the MT growth patterns (Figure 5A), including the numbers of EB1 comets emanating from the centrosome and the movement speed of the comets, using Imaris Lineage/Track software. We found that 9.86 ± 4.11 comets emanated from the centrosome every 5 s in siControl cells during the recording period. In contrast, 4.23 ± 2.37 comets/5 s emanated from the centrosome in siArl4D-treated cells (Figure 5B). This result indicates that depletion of Arl4D resulted in a defect in centrosomal MT nucleation. We also analyzed the velocity of EB1 comets moving in the cell; this velocity is an indicator of the MT polymerization rate. We found that depletion of Arl4D did not affect the growth rate of EB1 comets (0.255 ± 0.049 μm/s in siControl vs. 0.243 ± 0.041 μm/s in siArl4D-treated cells), indicating that the growth rate of MTs was not affected by Arl4D depletion (Figure 5C).

Using EB1-GFP, we also observed that the EB1 signal at the centrosome was reduced at the centers of MT asters in siArl4D-treated cells (Supplemental Movie S1). We therefore examined the endogenous EB1 signal in Arl4D-depleted cells (Figure 5D). We used siRNA to knock down Arl4D in COS-7 cells and stained the cells with EB1 and a centrosome marker (γ-tubulin). We found that the signal intensity of the EB1 signal at the centrosomes was reduced in Arl4D-depleted cells (Figure 5E). In contrast, knockdown of Arl4D did not affect p150 signal intensity at the centrosome (Figure 5F). Our findings thus demonstrated that Arl4D depletion results in less prominent aster formation; this effect could be attributed to the diminished MT nucleation from the centrosome. This diminished nucleation might be a result of reduced EB1 recruitment to the centrosome in Arl4D-depleted cells.

Disruption of the EB1–Arl4D interaction resulted in a centrosomal MT regrowth defect

The observations presented above indicated that Arl4D, like EB1, participates in the process of centrosomal MT regrowth. To investigate the importance of the EB1–Arl4D interaction in the MT regrowth process, we first attempted to identify motifs that are required for EB1–Arl4D interaction on either protein. The EBH domain of EB1 is known to interact with Sx(L/I)P motifs in proteins such as adenomatous polyposis coli (APC), CLIP-associated proteins (CLASPs), and MT-actin cross-linking factor (Honnappa *et al.,* 2009). Sequence alignment of Arl4 family proteins showed that Arl4D and Arl4A, but not Arl4C, contain SxLP motifs (Figure 6A), suggesting that Arl4D and Arl4A might interact with EB1 via their SxLP motifs. To examine whether the SxLP motif of Arl4D plays a role in Arl4D-EB1 interaction, we mutated the Arl4D SFLP motif (residues 14–17)

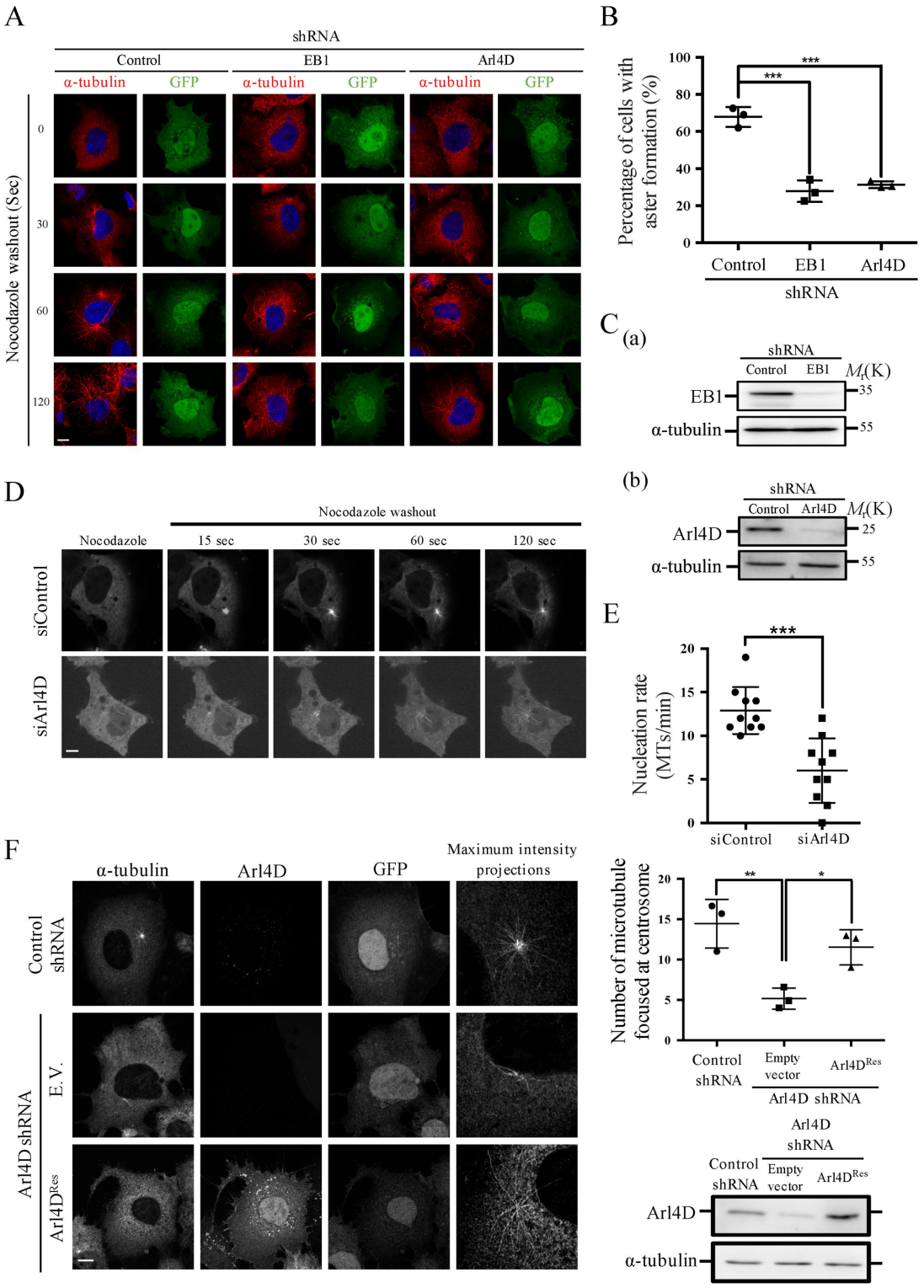

FIGURE 3: Arl4D knockdown results in a defect in aster formation during MT regrowth. (A) Immunofluorescence staining of cells at different time points during MT regrowth. COS-7 cells transfected with control, EB1, or Arl4D pSuper-shRNA (GFP-tag) for 72 h were processed for MT regrowth assays as described in *Materials and Methods*, and the cells were subsequently fixed at the indicated times. The cells were stained with DAPI (blue) and antibodies against α-tubulin (red). The GFP signal indicates transfected cells. Scale bars, 10 μm. (B) Quantification of cells with apparent centrosomal aster formation during MT regrowth. The percentages of cells with apparent centrosomal aster formation in each group were determined at 30-s intervals in 67–133 cells in each experiment. Normal aster formation is indicated by the presence of MT astral rays composed of 10 or more discernible fibers (or MTs). The experiment was repeated three times (total cells from three experiments: control shRNA = 361, EB1 shRNA = 264, and Arl4D shRNA = 279). The error bars represent SD. ***$P < 0.001$ by one-way ANOVA with Dunnett's post hoc multiple comparison

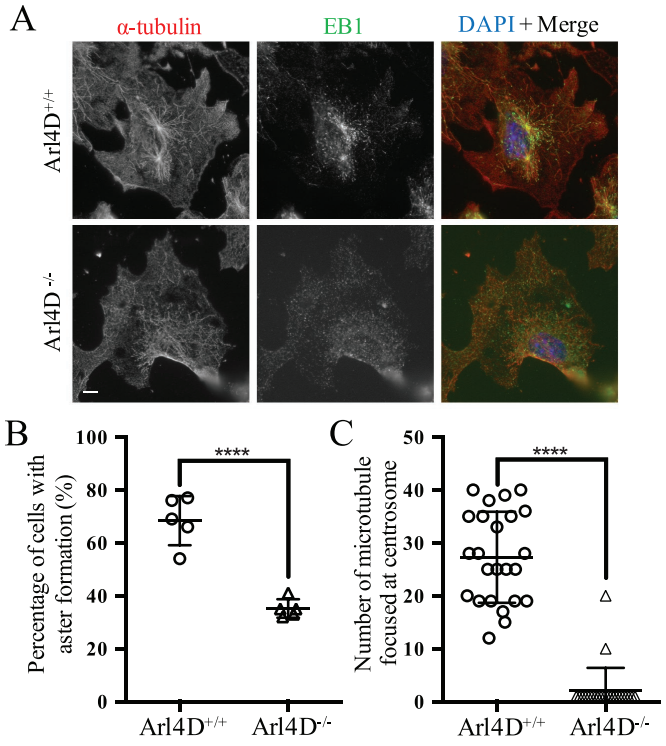

FIGURE 4: Arl4D-knockout MEFs shows a defect in aster formation during MT regrowth. MT regrowth assays were performed with $Arl4D^{+/+}$ and $Arl4D^{-/-}$ MEFs as described in *Materials and Methods*, and the cells were processed for immunofluorescence staining and labeled with anti-EB1, anti-α-tubulin, and DAPI (left). Scale bar, 10 μm. (B) Quantification of MEFs with centrosomal aster at 120 s; the data are shown as the mean ± SD from at least five experiments. Normal aster formation is indicated by the presence of MT astral rays composed of 10 or more discernible fibers (or MTs). ****$P < 0.0001$ by Student's *t* test. (C) Quantification of the numbers of MTs emanated from the aster during regrowth. The data are presented as mean ± SD (total cells $Arl4D^{+/+} = 30$, $Arl4D^{-/-} = 36$). ****$P < 0.0001$ by Student's *t* test.

to SFNK (Honnappa *et al.*, 2009) and performed co-immunoprecipitation assays. We first co-expressed GFP-EB1 protein with $Arl4D^{WT}$-Myc or $Arl4D^{NK}$-Myc in COS-7 cells and subjected the cell lysates to immunoprecipitation using GFP-Trap or Myc-Trap. As shown in Figure 6, B and C, introduction of the NK mutation in the SxLP motif of Arl4D resulted in a 20–43% decrease in the amount of protein co-immunoprecipitated in the GFP- and Myc-Trap assays. These results indicated that interaction between Arl4D and EB1 is partially dependent on the SxLP motif. Taken together, our findings show a canonical EBH-binding motif, SxLP, of Arl4D contributes to its interaction with EB1 (Figure 6D).

It is well known that the EBH domain is an important protein-interacting domain within EB1. We next employed an alanine scanning mutagenesis strategy to identify the amino acid residues required for Arl4D interaction within the EBH domain of EB1. We changed four to five of the amino acids within the EBH domain (aa 208–251) to Ala at a time and evaluated the interaction of a total of nine mutated EBH domains with Arl4D using the yeast two-hybrid assay (Figure 7A). The Ala-scan mutants A3, A4, and A7 showed decreased interaction with Arl4D. Structural analysis of the C-terminal region of EB1 has shown that residues 191–230 form a long, smoothly curved helix (α1) that is followed by an antiparallel short helix (α2, residues 237–248) connected to the first helix by a hairpin structure (Honnappa *et al.*, 2005). These helical structures form interacting grooves that are crucial for both the homodimerization of EB1 and its interaction with other proteins. The A3 and A4 mutations alter several amino acids that are known to affect EB1 oligomerization and function (Askham *et al.*, 2002; Bu and Su, 2003; Slep *et al.*, 2005). The A7 mutation resides in the α2 region of EB1 and is not on the surface of the interacting groove. No report to date has characterized the effect of altering these amino acids. We thus focused on the effect of the A7 mutation on EB1 function.

We examined the effect of the EB1-A7 mutation on the interaction of EB1 with Arl4D. In the context of the full-length EB1 protein, A7 mutant did not show interaction with Arl4D as determined by the yeast two-hybrid assay (Figure 7B). We next co-expressed Arl4D and either WT EB1 or the A7 mutant in COS-7 cells and subjected lysates of the cells to immunoprecipitation using GFP-Trap. As shown in Figure 7C, Arl4D co-immunoprecipitated with both the WT and the EB1-A7 proteins; however, the relative quantity of protein that co-immunoprecipitated with EB1-A7 was approximately 50% of the amount that co-immunoprecipitated with WT EB1 (Figure 7C), indicating that the A7 mutation reduced EB1's binding affinity for Arl4D. To rule out the possibility that the A7 mutation completely disrupts the conformation of EB1, we evaluated the effect of the A7 mutation both on the homodimerization of EB1 and on its interaction with other known proteins. We used one of two different tags (FLAG and GFP) in the WT and A7-mutant forms of EB1, expressed them in various combinations in HeLa cells, and performed immunoprecipitation using GFP-Trap. As shown in Figure 7D, FLAG-tagged EB1-A7 co-immunoprecipitated with the A7 mutant of GFP-tagged EB1,

test. (C) Decrease in EB1 or Arl4D protein levels after shRNA knockdown. Seventy-two hours after transfection with control, EB1, or Arl4D pSuper-shRNA, COS-7 cell lysates were analyzed by Western blotting with the indicated antibodies. (D) COS-7 cells stably expressing MT-BD of ensconsin (EMTB)-mCherry were transfected with control or Arl4D siRNA, and the cells were subjected to time-lapse live cell imaging as described in *Materials and Methods*. Representative time-lapse images collected from G1/S cells are shown. MT nucleation rates are presented as the average MT nucleation rate ± SD; $n = 10$ cells, siControl samples; $n = 10$ cells, siArl4D samples. Scale bar, 10 μm. (E) Quantification of MTs nucleation rates (MTs/min) during MT regrowth. The experiment was repeated three times (total cells from three experiments: siControl = 10, siArl4D = 10). The data are presented as mean ± SD. ***$P < 0.001$ by Student's *t* test. (F) Overexpression of shRNA-resistant Arl4D ($Arl4D^{Res}$) rescued the MT regrowth defect in COS-7 cells. COS-7 cells transfected with Arl4D pSuper-shRNA together with an empty vector or $Arl4D^{Res}$ DNA were fixed at 30 s after the start of the MT regrowth assay and stained with antibodies against Arl4D and α-tubulin (left panel). Scale bars, 10 μm. Top right, quantification of the numbers of MTs emanated from the aster during regrowth. The numbers of MTs were estimated as described in *Materials and Methods*. The data shown are the mean ± SD from at least three experiments (total cells from three experiments: control shRNA = 60, Arl4D shRNA = 58, and Arl4D shRNA with $Arl4D^{Res}$ = 52). *$P < 0.05$. **$P < 0.01$ by one-way ANOVA with Dunnett's post hoc multiple comparison test. Bottom right, Western blot analysis of cell lysates from COS-7 cells transfected with the indicated shRNA and plasmids.

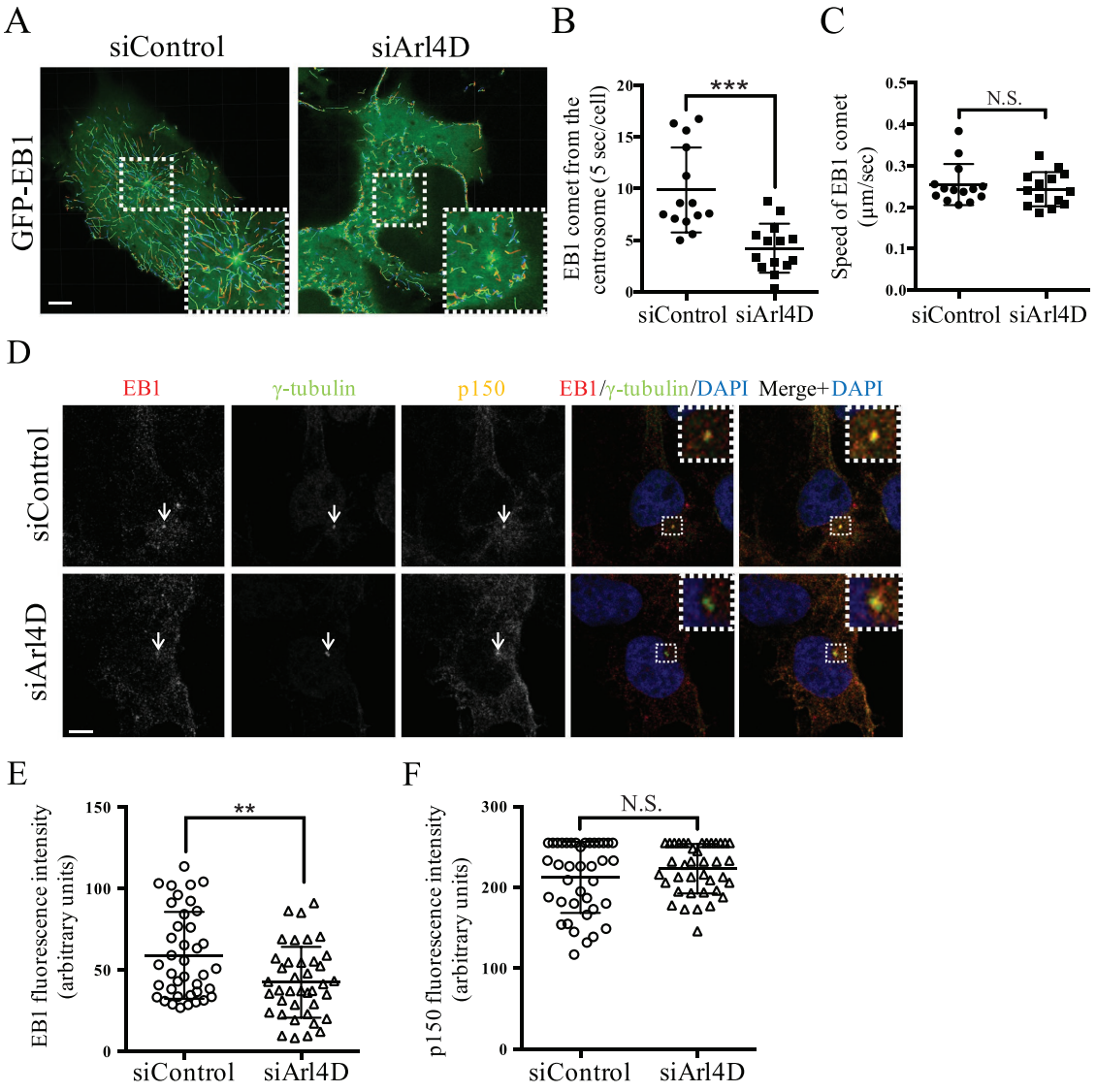

FIGURE 5: Arl4D is involved in normal MT growth and in the centrosomal recruitment of EB1. (A–C) Time-lapse microscopy of siControl- and siArl4D-treated COS-7 cells expressing low levels of GFP-EB1 was performed as described in *Materials and Methods* and the video is presented in Supplemental Movie S1. (A) Representative images of tracked EB1-GFP comet trajectories during a 120-s time interval under control and knockdown conditions in COS-7 cells. (B) An automated tracking program (Imaris Lineage/Spots) was used to calculate the number of EB1 comets starting from the centrosome, (9.86 ± 4.11 comets from centrosome/5 s vs. 4.23 ± 2.37 comets from centrosome/5 s in siControl vs. siArl4D cells) ($n = 14$ cells per experiment from three independent experiments, error bars represent the SD. ***$p < 0.001$ by Student's *t* test). (C) Using an automated tracking program (Imaris Lineage/Track), to track EB1 comets, we found that the comet speed in Arl4D-depleted cells was not significantly different from that in control cells (0.255 ± 0.049 μm/s vs. 0.243 ± 0.041 μm/s, siControl vs. siArl4D) ($n = 14$ cells per experiment from three independent experiments, error bars represent mean ± SD. N.S., $p > 0.05$ by Student's *t* test). (D) COS-7 cells were transfected with siControl or siArl4D, and cells were processed for immunofluorescence staining and labeled with anti-EB1 (red), anti-γ-tubulin (green), anti-p150 (yellow), and DAPI (blue). Scale bar, 10 μm. (E) Quantification of EB1 fluorescence intensity at centrosome in COS-7 cells ($n = 39$ centrosomes, error bars represent mean ± SD; **$p < 0.01$ by Student's *t* test). (F) Quantification of p150 fluorescence intensity at centrosome in COS-7 ($n = 39$ centrosomes. The error bars indicate the SD. N.S., $p > 0.05$ by Student's *t* test).

indicating that mutation in the A7 region did not affect EB1 homodimerization and that the EB1-A7 protein retained some if not all of its structural characteristics. CLASP2, an EB1-interacting protein that is required for MT formation from the trans-Golgi network (Efimov *et al.*, 2007), also remained bound to the EB1-A7 mutant (Figure 7E). Taken together, these results indicated that the EB1 A7 mutant largely retained its structural integrity.

We next examined whether the A7 mutation affects the ability of EB1 to promote MT nucleation from the centrosome after nocodazole-induced MT depolymerization and washout. We expressed siRNA-resistant WT EB1 (EB1-WT^{Res}) and the A7 mutant (EB1-A7^{Res}) in COS-7 cells treated with EB1 siRNA (Figure 8A). The expression levels of exogenous EB1s in the rescue experiment were approximately 3- to 5-fold higher than that of endogenous EB1. Depletion

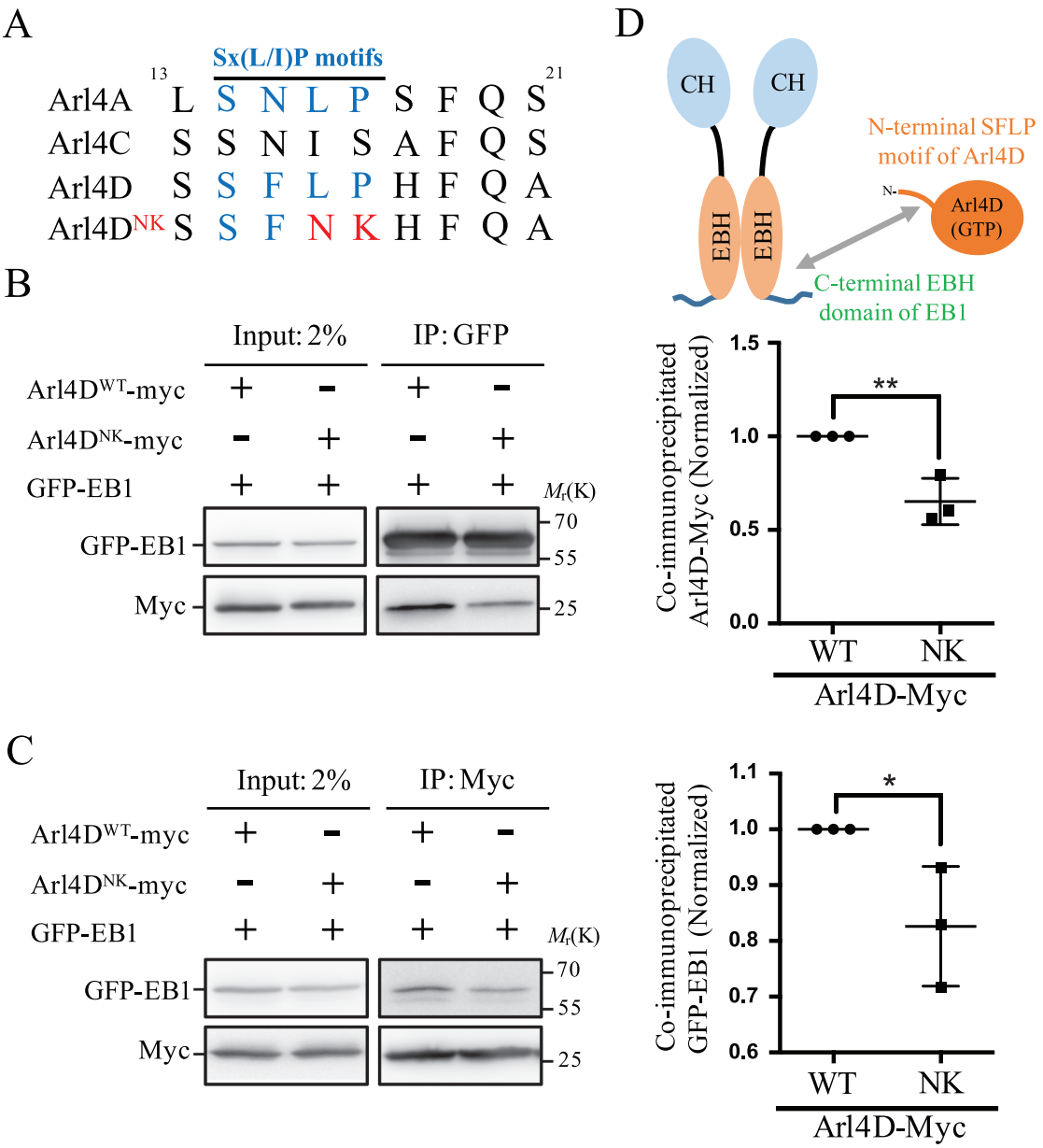

FIGURE 6: The SxLP motif in the Arl4D N-terminal region stabilizes the EB1–Arl4D interaction. (A) Conservation of the Sx(L/I)P motif in Arl4 family members. Sequence alignment of Arl4 family proteins showed that Arl4D and Arl4A, but not Arl4C, contain Sx(L/I)P motifs. The Sx(L/I)P motif is shown in red. (B) Interaction of EB1 with Arl4D was disrupted after mutagenesis of the SFLP motif (residues 14–17). Lysates of COS-7 cells transfected with plasmids encoding GFP-EB1 and Arl4D^{WT}-Myc or Arl4D^{NK}-Myc were immunoprecipitated with GFP-Trap, and the immunoprecipitated proteins were analyzed by Western blotting with antibodies against Myc and GFP. The amounts of co-immunoprecipitated Arl4D-myc were determined by densitometric quantification of the results of four experiments. The data are presented as mean ± SD. $^{**}P < 0.01$ by Student's *t* test. (C) Lysates of COS-7 cells transfected with plasmids encoding GFP-EB1 and Arl4D^{WT}-Myc or Arl4D^{NK}-Myc were immunoprecipitated with Myc-Trap, and immunoprecipitated proteins were analyzed by Western blotting with antibodies against Myc and GFP. The amounts of co-immunoprecipitated GFP-EB1 were determined by densitometric quantification from four experiments. The data are presented as mean ± SD. $^{**}P < 0.05$ by Student's *t* test. (D) Cartoon illustrating how Arl4D interacts with EB1 through the latter's EBH domain in a GTP-dependent manner; a canonical EBH-binding motif, SxLP, of Arl4D contributes to its interaction with EB1.

of EB1 significantly reduced the number of MTs emanating from the centrosome; an average of 11 ± 1.3 MTs/ aster was observed in control cells while the number in EB1 knockdown cells was 4.8 ± 0.8. In EB1-depleted cells overexpressing GFP, the average number was 4.0 ± 0.8 MTs/aster. In cells overexpressing EB1-WT^{Res} or EB1-A7^{Res}, the numbers were 9.4 ± 0.9 and 4.5 ± 0.1 MT/aster, respectively (Figure 8B). These results indicate that the A7 mutation of EB1 is defective in promoting MT nucleation. We also examined whether the centrosomal recruitment of EB1 is affected by the A7 mutation. We expressed GFP-EB1-WT^{Res} and GFP-EB1-A7^{Res} in EB1-depleted COS-7 cells and found that the signal intensity of GFP-EB1-A7 at the centrosome was reduced (Figure 8, C and D). Together, these results indicate that Arl4D binding to EB1 is important for the centrosomal recruitment of EB1 and MT nucleation at the centrosome.

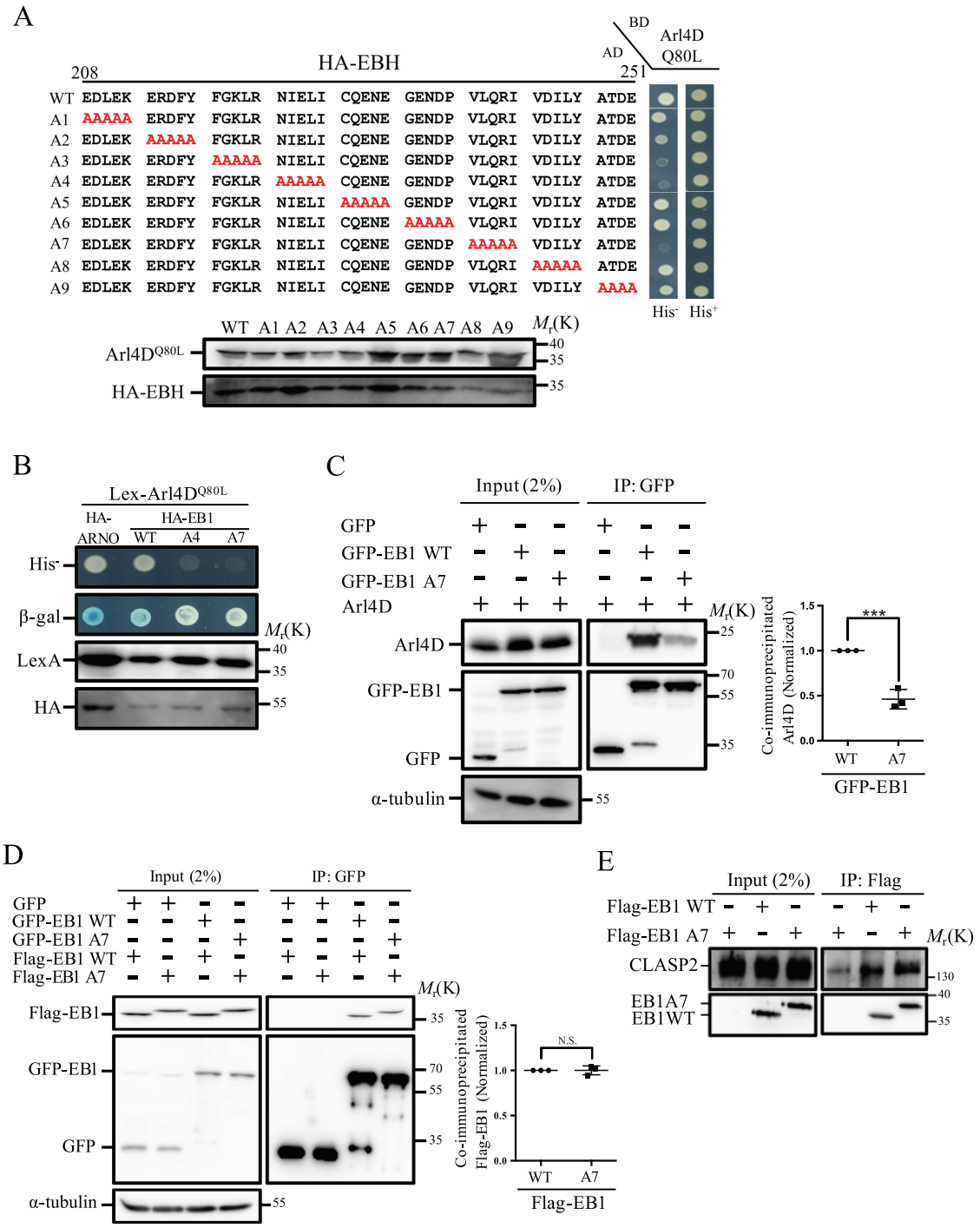

FIGURE 7: Characterization of Arl4D-binding-defective EB1 Ala-scanning mutant. (A) Identification Arl4D-binding-defective EB1 mutant. A schematic representation of the alanine-scanning mutagenesis performed in the EB1 EBH domain is shown at the top left. Four to five amino acids at a time were replaced with Ala in the EB1 EBH fragments (aa 208–251). Interactions of Arl4D^{Q80L} with the EBH alanine-scanning mutants A1-A9 were tested using the yeast two-hybrid assay as described in *Materials and Methods*. The histidine auxotrophy and protein expression levels are shown in the left and bottom panels, respectively. EBH A3, A4, and A7 mutants disrupted the Arl4D^{Q80L}-EBH interaction. (B) Confirmation of an Arl4D-binding defect in the EB1 A4 and A7 mutants. Full-length EB1 with A4 or A7 mutation could not interact with Arl4D^{Q80L} in the yeast two-hybrid assay. Histidine auxotrophy, β-galactosidase activity, and protein expression level are shown. (C) The A7 mutant of EB1 does not interact with Arl4D^{WT} in vivo. Co-immunoprecipitation of EB1 and Arl4D were assessed from lysates of COS-7 cells expressing the indicated combinations of Arl4D and GFP-EB1 constructs were assessed. The bound proteins were analyzed by Western blotting with antibodies against GFP, Arl4D, and α-tubulin (left). Right: densitometric quantification of co-immunoprecipitated Arl4D. The data shown are the mean ± SD from three experiments. ***$P < 0.001$ by Student's *t* test. (D) Homodimerization of EB1-A7 mutant in vivo. Lysates of COS-7 cells transfected with the indicated plasmids were

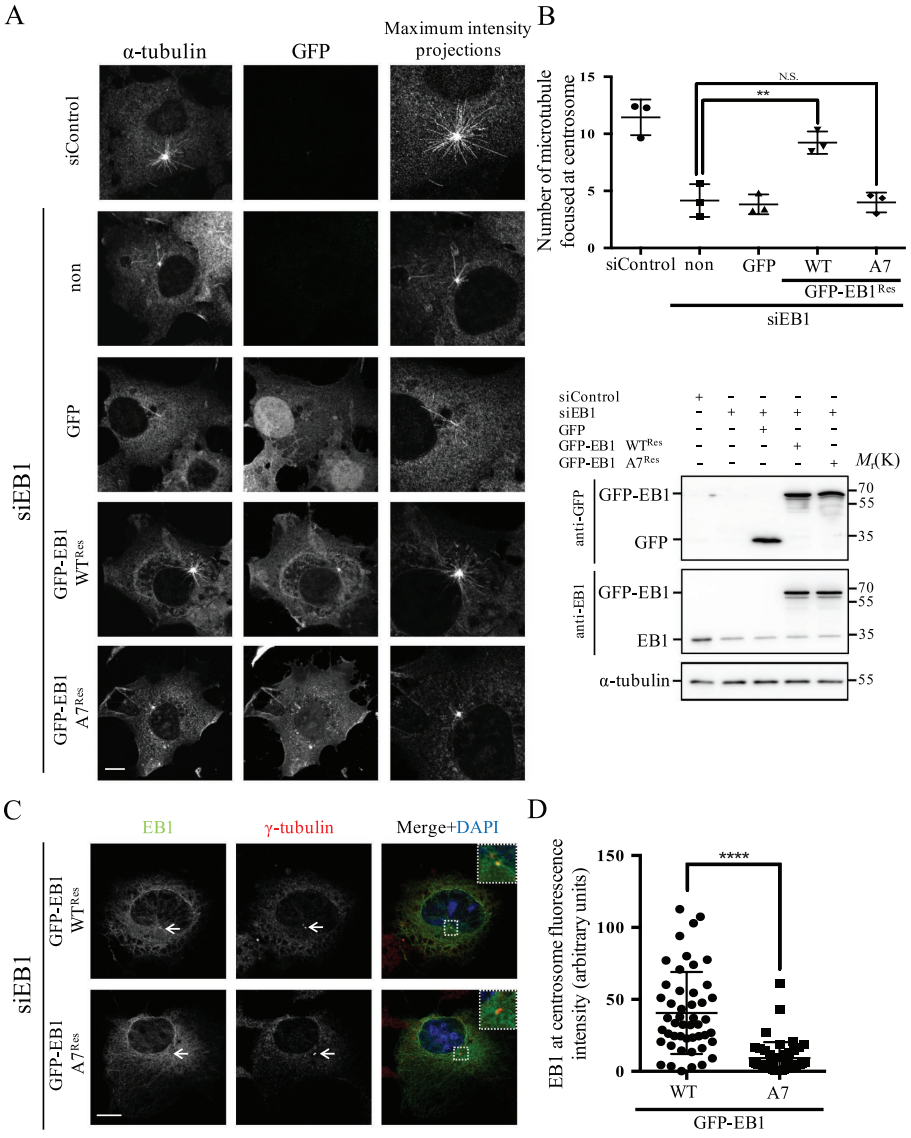

FIGURE 8: The A7 mutation of EB1 displays a defect in MT regrowth and diminished centrosomal localization. (A) MT regrowth assay of EB1-knockdown cells expressing GFP-EB1, GFP-EB1-A7, or GFP. COS-7 cells were transfected with control or EB1 siRNA together with N-terminal GFP-tagged EB1 siRNA-resistant constructs, wild-type (GFP-EB1 WT^{Res}) or A7 mutant (GFP-EB1-A7^{Res}). Cells were fixed after 30 s of MT regrowth and stained with antibodies against α-tubulin. Scale bars, 10 μm. (B) Top panel: quantification of the numbers of MTs emanating from the centrosome during regrowth. The data are mean ± SD. The experiment was repeated three times (total cells from three experiments: control siRNA = 37, siEB1 = 47, siRNA EB1 with GFP = 45, siRNA EB1 with GFP-EB1 WT^{Res} = 38 and siRNA EB1 with GFP-EB1-A7^{Res} = 43). $^{**}P < 0.01$ by one-way ANOVA with Dunnett's post hoc multiple comparison test. Bottom panel, expression levels of the transfected constructs. Lysates of cells used in A were analyzed by Western blotting with antibodies against EB1, GFP and α-tubulin. (C) EB1-A7 mutant showed decreased centrosomal localization. COS-7 cells were transfected with EB1 siRNA together with GFP-EB1 WT^{Res} or GFP-EB1-A7^{Res}, and cells were processed for immunofluorescence staining and labeled with anti-γ-tubulin (red) and DAPI (blue). Scale bar, 10 μm. (D) Quantification of GFP-EB1 fluorescence intensity at the centrosome in COS-7 ($n = 48$ centrosomes, error bars indicate SD. $^{****}P < 0.0001$ by Student's t test).

Arl4D modulates the association of EB1 with p150

A previous report indicated that the formation of radial MT arrays from the centrosome requires interaction between EB1 and p150 (Askham *et al.*, 2002; Hayashi *et al.*, 2005; Strickland *et al.*, 2005). We therefore examined whether the interaction between EB1 and p150 is affected by the EB1-A7 mutation. Lysates from HeLa cells expressing either GFP-tagged EB1 WT or the A7 mutant were subjected to immunoprecipitation using GFP-Trap, and co-immunoprecipitated proteins were analyzed by immunoblotting. As shown in Figure 9A, the WT form but not the A7 mutant form of EB1 interacted with p150. Although this result might indicate that the interaction of EB1 with Arl4D is important for the EB1–p150 interaction, it also raises the possibility that EB1-A7 led to impaired MT regrowth simply because it lost its ability to bind to p150. To rule out that possibility, we examined the interaction between WT EB1 and p150 in Arl4D-knockdown cells. Lysates of HeLa or C-33A cells treated with Arl4D or control siRNA and overexpressing GFP-EB1 or GFP were subjected to immunoprecipitation using GFP-Trap. The amount of p150 co-immunoprecipitated with GFP-EB1 was reduced (30–40%) in Arl4D siRNA-treated cells compared with that in control cells. The interaction between GFP-EB1 and p150 was restored when we overexpressed the siRNA-resistant form of Arl4D protein (Figure 9, B and C). These results provide further evidence that the interaction between Arl4D and EB1 may play a role in stabilizing EB1–p150 interaction.

DISCUSSION

In this study, we identified EB1 as a functional partner of Arl4D. We found that Arl4D interacts with EB1 in a GTP-dependent manner, colocalizes with γ-tubulin, and modulates MT nucleation by recruiting EB1 to the centrosome. Depletion of Arl4D interfered with EB1 localization to the centrosome and resulted in decreased numbers of MT growing from the centrosome. Thus, we propose that Arl4D promotes centrosomal recruitment of EB1 via direct interaction, thereby modulating MT growth at the centrosome.

immunoprecipitated with a GFP antibody, and the bound proteins were analyzed by Western blotting with antibodies against GFP and FLAG (left). Right: quantification of co-immunoprecipitated FLAG signals. The data shown are the mean ± SD from three experiments; no significant difference was found. (E) Interaction of EB1 with CLASP2 was not affected by the A7 mutation. Lysates of COS-7 cells transfected with the indicated plasmids were immunoprecipitated with FLAG antibody, and bound proteins were analyzed by Western blotting with antibodies against CLASP2 and FLAG.

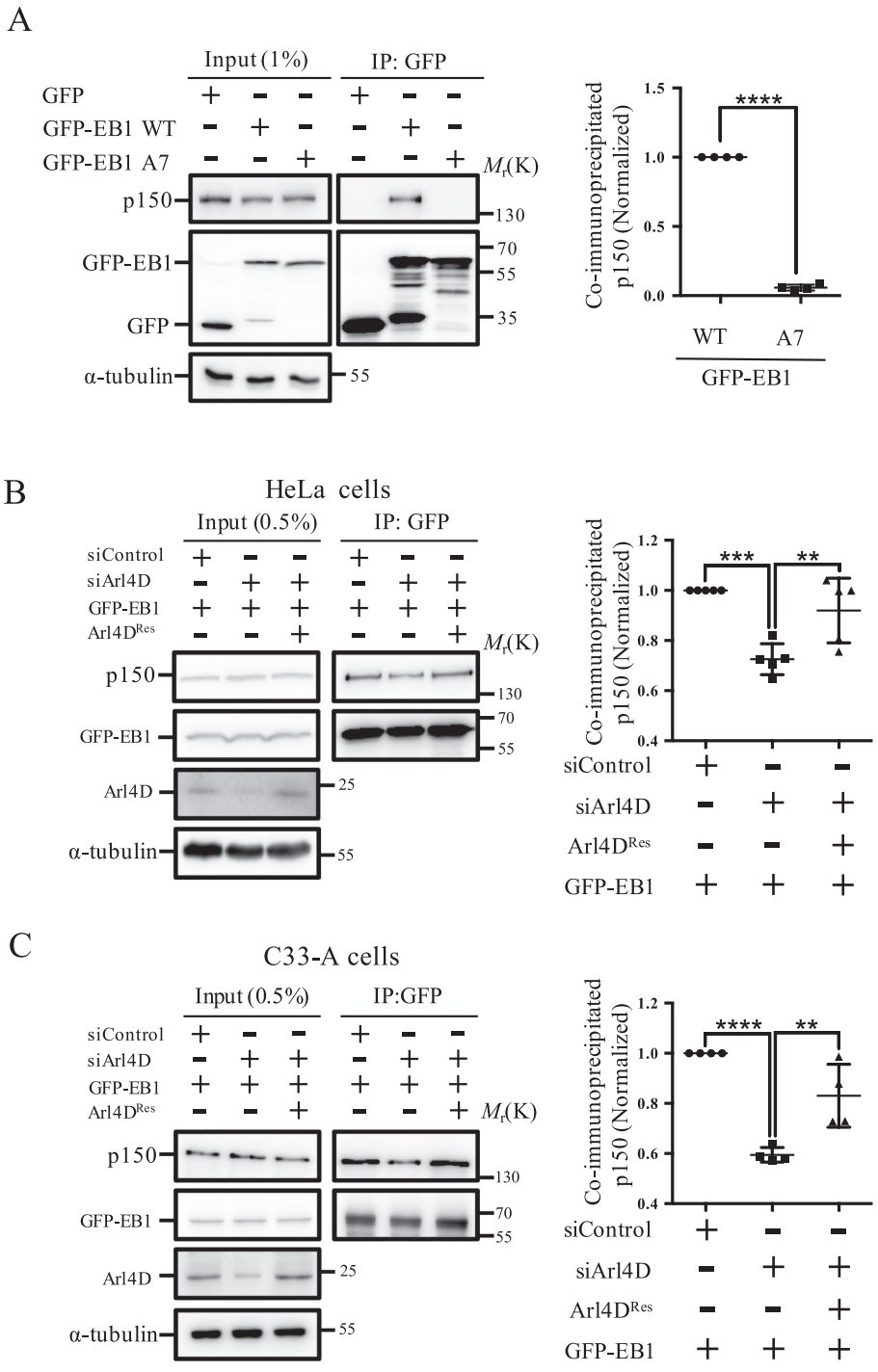

FIGURE 9: Arl4D binding to EB1 regulates the association of EB1 with p150. (A) Interaction of EB1 with p150 was disrupted after mutagenesis in the EBH A7 region. Lysates of HeLa cells transfected with plasmids encoding GFP, GFP-EB1 wild-type, or A7 mutants were immunoprecipitated with GFP-Trap, and immunoprecipitated proteins were analyzed by Western blotting with antibodies against p150, GFP, and α-tubulin. The amounts of co-immunoprecipitated p150 were determined by densitometric quantification from four experiments. The data are presented as mean ± SD. ****$P < 0.0001$ by Student's *t* test. (B) Effects of Arl4D knockdown on the EB1 interaction with p150 were rescued by overexpression of Arl4D^{Res} in HeLa cells. Lysates of cells transfected with control or specific Arl4D siRNA as well as with the indicated plasmids were immunoprecipitated with GFP-Trap, and the bound proteins were analyzed by Western blotting with the indicated antibodies. The amounts of co-immunoprecipitated p150 in five experiments were determined by densitometric quantification. The data are presented as mean ± SD. **$P < 0.01$, ***$P < 0.001$ by one-way ANOVA with Dunnett's post hoc multiple comparison test. (C) Effects of Arl4D knockdown on the EB1 interaction with p150 were rescued by overexpression of Arl4D^{Res} in C33-A cells. Lysates of cells transfected with control or specific Arl4D siRNA as well as the indicated plasmids were immunoprecipitated with GFP-Trap, and bound proteins were analyzed by Western blotting with the indicated antibodies. Amounts of co-immunoprecipitated p150 were determined by densitometric quantification from four experiments. The data are presented as mean ± SD. **$P < 0.01$, ****$P < 0.0001$ by one-way ANOVA with post hoc multiple comparison test.

Like many other ARF family members, Arl4D protein has been shown to localize to several different cellular compartments, including the plasma membrane, nucleus, and mitochondria, and is also distributed throughout the cytosol (Lin *et al.*, 2002, 2007, 2012). In this report, we observed endogenous Arl4D localized at the centrosome. Previously, HP1α, a protein that localizes to the centrosome (Auth *et al.*, 2006), was reported to interact with Arl4D (Lin *et al.*, 2002). Auth *et al.* (2006) found that HP1α depletion could impede cell cycle progression, lead to the formation of multinucleated cells, and result in less well-organized MT networks (Auth *et al.*, 2006). These findings are consistent with our current evidence that Arl4D might localize to the centrosome and may participate in MT-related centrosomal function.

How does Arl4D affect MT growth from the centrosome? Our current findings suggest that Arl4D modulates MT nucleation via its interaction with EB1. Arl4D interacts with EB1 in a GTP-dependent manner through the latter's EBH domain. A canonical EBH-binding motif, SFLP (SxI/LP), was found in the N-terminal region of Arl4D. Interestingly, mutating the Arl4D SxI/LP motif only partially reduced Arl4D binding to EB1. This result suggests that there are other EB1-binding site(s) within Arl4D that remain to be characterized.

Depletion of either EB1or Arl4D resulted in similar MT regrowth defects: the formation of MT asters on MT regrowth from the centrosome after MT depolymerization was impeded in EB1- or Arl4D-depleted cells. We also found that the numbers of MTs nucleating from the centrosome at early time points during MT regrowth were decreased in Arl4D-depleted cells as well as in cells in which the interaction between Arl4D and EB1 was disrupted. These findings established a role for Arl4D-EB1 interaction in MT regrowth from the centrosome. In our time-lapse imaging experiments, we found that

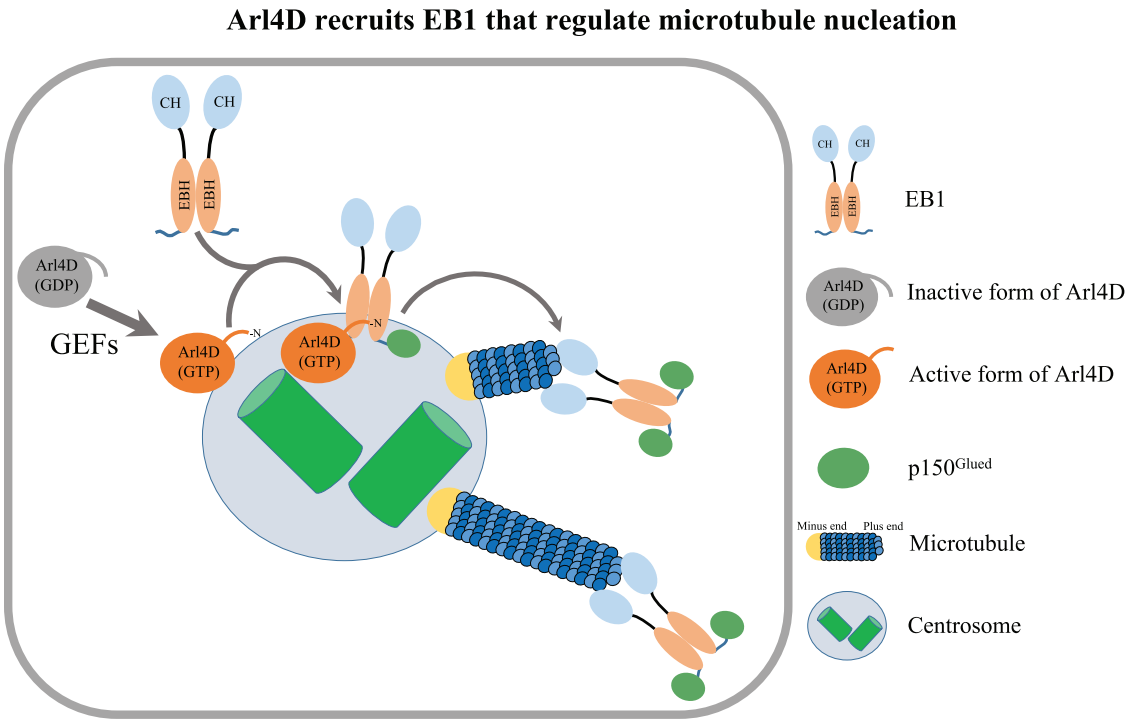

FIGURE 10: Model showing how Arl4D modulation of EB1 function affects MT growth. The activated GTP-bound form of Arl4D is localized at the centrosome and interacts with EB1 at its C-terminal EBH domain. Arl4D binding to EB1 results in centrosomal recruitment of EB1. EB1 interacts with $p150^{Glued}$ to form a complex with MTs, thereby promoting MT growth.

the number of MTs growing from the centrosome and the number of EB1 comets emanating from the centrosome were reduced in Arl4D-depleted cells. However, the velocity of EB1 comets was not affected by Arl4D depletion, indicating that the rate of MT polymerization was not affected. The effect of Arl4D depletion on centrosomal MT nucleation is apparent. However, it is rather difficult to distinguish between MT nucleation and anchoring, even with live cell imaging. Since the ratio of emanating MTs observed by time-lapse imaging in siArl4D verses control cells was larger than the ratio we observed in still images, we could not completely exclude the possibility that there is an MT-anchoring defect in Arl4D-depleted cells.

The nucleation and minus end anchoring of MTs are dependent on two EB1-interacting proteins, APC and p150 (Askham *et al.*, 2002; Louie *et al.*, 2004). Mutations that interfered with EB1–Arl4D binding also affected EB1–p150 binding, and this might, in turn, contribute to the MT regrowth defect observed in this study. EB1 interacts with p150 through a composite of its EBH domain and its C-terminal EEY motif (Askham *et al.*, 2002; Bu and Su 2003; Slep *et al.*, 2005). The EBH domain is also the region we identified as the Arl4D binding region. Thus one could argue that mutations within the EBH domain (such as the A7 mutant characterized in this study) simply abolished EB1's interaction with all of its binding partners. Several lines of evidence suggest that the aforementioned scenario might not be true. Secondary structure prediction data suggest that mutation of the A7 region does not affect the EB1 α2 helix structure (Slep *et al.*, 2005). Protein structure model prediction also indicated that mutation of this region only slightly changed the conformation of the EB1 α2 helix (Supplemental Figure S4). In our report, we found that neither EB1 homodimerization nor its interaction with CLASP2, a protein responsible for noncentrosomal MT nucleation at the Golgi membrane (Efimov *et al.*, 2007), was affected by A7 mutation. Interestingly, knockdown of Arl4D did not affect p150 signal intensity at the centrosome, suggesting that Arl4D is not involved in the centrosomal recruitment of p150. Thus, the interaction between EB1 and p150, albeit direct, might be further modulated by Arl4D. Understanding the interplay among Arl4D, EB1, and p150 will greatly foster our understanding of the mechanisms of MT regrowth. In various experimental systems it is suggested that EB1 may also contribute to MT nucleation directly or via recruitment of other factors, such as APC, XMAP215, or γ-tubulin ring complex (Nakamura *et al.*, 2001; Zanic *et al.*, 2013; Bouissou *et al.*, 2014). Whether Arl4D also plays a role in the formation of other EB1-complexes remains to be further investigated.

Based on our findings, we propose a model in which the activated, GTP-bound form of Arl4D localizes to the centrosome and interacts with EB1 in such a way as to facilitate the recruitment of EB1 to the centrosome, where it binds to p150 and initiates MT nucleation (Figure 10). We speculate that after forming complexes with p150 to initiate centrosomal MT growth, the conformation of EB1 might be changed and that a putative GTPase-activating protein (GAP) promotes GTP hydrolysis of Arl4D so that Arl4D dissociates from EB1. The free Arl4D protein can then recycle, undergo activation, and interact with additional EB1 molecules to initiate the nucleation of new MT growth at the centrosome. In the absence of Arl4D, less EB1 is recruited to the centrosome and its binding to p150 is also weakened. Our model suggests that Arl4D does not remain in a complex with EB1 but instead leaves the complex on initiation of MT nucleation; hence, no decoration of MT plus ends by Arl4D was observed. However, further studies will be required to test this hypothesis.

Arf small GTPases are controlled by the stimulation of the release of bound GDP by GEFs and by stimulation of their intrinsic GTPase activity by GAPs (Donaldson and Jackson, 2011; Sztul *et al.*, 2019). Our study found that Arl4D functions and interacts with EB1 in a nucleotide-dependent manner, suggesting that a putative GEF and GAP associated with Arl4D play important roles in regulating the interaction between Arl4D and EB1. Identification of molecules that act upstream of Arl4D, such as Arl4D GAPs and GEFs, is of great importance in further exploration of the detailed mechanism of Arl4D action.

We have previously reported that another Arl4 member, Arl4A, binds to a coiled-coil region of GCC185 (Lin *et al.*, 2011) and strengthens the recruitment of CLASP proteins to the Golgi. MT depolymerization and regrowth from the centrosome were not affected in Arl4A-depleted cells (unpublished data); however, the Golgi morphology was disturbed, possibly due to a defect in Golgi-derived MT formation. It is interesting that two closely related Arl4 proteins appear to modulate MT dynamics at two different MT nucleation sites. It is also worth noting that these proteins appear to function in a similar manner by modulating the strength of intermolecular interactions between their effectors.

Three other Arl proteins, Arl2, Arl3, and Arl6, have been shown to localize to the centrosome (Zhou *et al.*, 2006; Wiens *et al.*, 2010). Depletion of Arl3 in cells leads to increased α-tubulin acetylation and failure of cytokinesis. Studies have suggested that Arl3 may be important in MT destabilization. Arl2 is thought to regulate MT assembly at the centrosome. Cells overexpressing $Arl2^{Q70L}$ failed to form MT asters from the centrosome in the MT regrowth assay (Zhou *et al.*, 2006). In contrast, we found that loss of Arl4D activity due to depletion of Arl4D resulted in reduced amounts of centrosomal MT nucleation. Whether these two molecules play antagonistic roles in fine-tuning centrosomal MT dynamics warrants further study. A previous study suggested that Arl6 localizes near the cilia and regulates their assembly and disassembly (Jin *et al.*, 2010; Wiens *et al.*, 2010). The localization of Arl6 is very similar to that of Arl4D: it colocalizes with γ-tubulin throughout the cell cycle (Wiens *et al.*, 2010). Our preliminary data showed that Arl4D-knockout MEFs displayed a minor defect in cilia formation. Whether Arl4D has a role in cilia formation needs further investigation.

In summary, our current study identified a centrosome-related role for Arl4D protein. Analysis of "upstream" regulators of Arl4D that underlie its selective recruitment to and activity at the centrosome will improve our understanding of the mechanism of Arl4D in regulating centrosomal MT growth. Recent studies indicate that the centrosome serves not only as an MTOC but also as a coordination center where important decisions concerning cell fate are made. Future studies examining whether Arl4D also participates in these processes will shed more light on the physiological roles of this protein.

MATERIALS AND METHODS

Cell culture, transfection, and antibodies

COS-7 and HeLa cells were grown in DMEM (Life Technologies, Lombard, IL) supplemented with 100 U/ml each of penicillin and streptomycin (Invitrogen) and 10% fetal bovine serum (FBS; Life Technologies). C33-A cells were grown in alpha minimum essential medium (MEM; HyClone) supplemented with 100 U/ml each of penicillin and streptomycin (Invitrogen), sodium pyruvate (Life Technologies), MEM nonessential amino acids (Life Technologies), and with 10% FBS (Life Technologies). The MEFs from both $Arl4D^{+/+}$ and Arl4D-knockout ($Arl4D^{-/-}$) mice were provided by the Transgenic Mouse Models Core Facility of the College of Medicine at National Taiwan University. MEFs were grown in DMEM (Life Technologies, Lombard, IL) supplemented with 10% FBS (Life Technologies). Arl4D expression levels were detected by Western blotting (Supplemental Figure S3).

Transient transfections were performed using Lipofectamine 2000 reagent (Invitrogen) according to the manufacturer's instructions. For the expression of Arl4D proteins in cells, cDNA of Arl4D was constructed as described previously (Li *et al.*, 2012). For knockdown of Arl4D and EB1, we used the pSuper RNAi system (OligoEngine) to specifically knock down gene expression. The sequences used to knock down these genes were as follows: Arl4D, 5′-GGTGGAGTTGCACCGAATC-3′ and EB1, 5′-TTGCCTTGAAGAAAGTGAA-3′. Forty-eight hours after transfection, the levels of the siRNA-targeted protein were analyzed by Western blotting. The EB1-GFP WT, A7, WT^{Res}, and $A7^{Res}$ forms were expressed under a CMV promoter in a pEGFP-C1 backbone. The FLAG-tagged EB1 WT and A7 mutant were expressed under a CMV promoter in a pCMV-Tag 2B backbone. The RNAi-resistant clone contained silent point mutations in the RNAi target sequence that decrease siRNA binding to the mRNA. A schematic representation of RNAi-resistant clone design and the mutation sites is presented in Supplemental Figure S5.

The antibodies used in this study were as follows: anti-EB1 (BD Transduction Laboratories), anti-HA (Invitrogen), anti-LexA (Covance), anti-CLASP2 (Absea Biotechnology), anti-FLAG M2 (Sigma-Aldrich), anti-GFP (Santa Cruz), anti-α-tubulin (Sigma-Aldrich), and anti-γ-tubulin (Sigma-Aldrich). The Arl4D antibodies were prepared by immunizing rabbits with Arl4D peptide (amino acid ^{139}QPGALSAAEVEKRLAVR^{155}). The Arl4A and GFP antibodies have been described previously (Li *et al.*, 2007, 2012; Lin *et al.*, 2011).

Protein interaction assays

Yeast two-hybrid assay. The yeast strain L40 (MATα trp1 leu2 his3 LYS 2::(lexAop)4-HIS3 URA3::(lexAop)8-lacZ) was constructed with two readouts for an interaction of histidine auxotrophy and β-galactosidase expression with the use of the LexA DNA-BD and GAL4-activation domain system. Yeast two-hybrid assays were performed as described previously (Li *et al.*, 2007). For expression of LexA DNA-BD fusion proteins in yeast, cDNAs of Arl4A (WT, Q79L and T34N), Arl4C (WT, Q72L and T27N), Arl4D (WT, Q80L and T35N), and lamin were cloned into a pBTM116 vector as described previously (Li *et al.*, 2007).

GST pull-down assay. For the expression of GST-fusion proteins in *Escherichia coli*, EB1 and its deletion mutants were cloned into pGEX vectors (GE Healthcare). For production of GST fusion protein, the indicated constructs were transformed into BL21. Colonies expressing recombinant proteins were grown at 37°C in Luria-Bertani medium. Protein expression was induced by the addition of 0.5 mM isopropyl β-D-1-thiogalactopyranoside for 3 h at 37°C. The cell pellet was incubated with lysozyme followed by sonication and centrifugation at 14,000 × *g* for 20 min to separate the soluble fraction (supernatant) from the insoluble fraction (pellet). The supernatant was incubated with glutathione Sepharose 4B beads (Amersham Pharmacia Biotech) at 4°C for 3 h. The beads were washed five times with cold phosphate-buffered saline (PBS) and then bound proteins were quantified by SDS–PAGE. Transfected COS-7 cells were lysed with RIPA buffer. The lysates were incubated with 10 μg of purified GST, GST-EB1, and GST-EB1-deletion mutants immobilized on glutathione beads for 3 h at 4°C. The beads were then washed three times with RIPA buffer, and the bound protein was analyzed by Western blotting.

Co-immunoprecipitation. COS-7 cells were lysed in lysis buffer (10 mM Tris-HCl, pH 7.5; 150 mM NaCl; 2 mM EDTA; 1% Triton X-100; protease inhibitor mixture) at 4°C for 30 min. The lysates were clarified by centrifugation at 15,000 × *g* for 30 min and incubated with primary antibodies at 4°C for 4 h with rotation. Then, the antibody-captured proteins were precipitated by protein G (Invitrogen). The co-immunoprecipitated proteins were analyzed by Western blotting. COS-7, HeLa, and C33-A cells were lysed in lysis buffer (10 mM Tris-HCl, pH 7.5; 150 mM NaCl; 0.5 mM EDTA; 0.5% NP40; protease inhibitor mixture) at 4°C for 30 min. The lysates were clarified by centrifugation at 15,000 × *g* for 30 min and incubated with GFP-Trap or Myc-Trap (ChromoTek) at 4°C for 1 h with rotation. The co-immunoprecipitated proteins were analyzed by Western blotting.

For examination of endogenous EB1 and Arl4D interaction, COS-7 cells were transfected with Arl4D. After 24 h, the cells were washed twice with cold PBS/Ca/Mg (PBS with $CaCl_2$ 0.1 mM and $CaCl_2$ 1 mM) and treated with 1 mM dithiobis (succinimidyl propionate) (DSP; Pierce Chemical, Rockford, IL) on ice for 2 h. After 2 h, the DSP was inactivated using 20 mM Tris, pH 7.4 in PBS/Ca/Mg and the cells were lysed in lysis buffer (10 mM HEPES, 150 mM NaCl, 1 mM EGTA, 0.1 mM $MgCl_2$, 0.5% Triton X-100, and protease inhibitor mixtures). The lysates were cleared by centrifugation 15,000 × *g* for 30 min at 4°C.

Western blotting. Cell lysates were prepared in RIPA buffer (50 mM Tris-HCl, pH 7.4; 150 mM NaCl; 1% NP-40; 0.5% SDS; 50 µg/ml Nα-p-tosyl-L-lysine chloromethyl ketone; 1 mg/ml benzamidine) and protease inhibitor mixture (Sigma-Aldrich), and protein concentrations were determined using a Bio-Rad protein assay (Bio-Rad). The protein samples were separated by SDS–PAGE and transferred to PVDF membranes (Millipore). After being probed with antibodies, the membranes were developed with the ECL system (Amersham-Pharmacia Biotech) according to the manufacturer's instructions and imaged on an ImageQuant LAS 4000 biomolecular imager. The bands of protein were quantified by ImageJ software.

MT regrowth assay

COS-7 cells were grown on coverslips and treated with 100 ng/ml nocodazole for 3 h at 37°C. The nocodazole was washed out, and the cells were incubated on ice for 30 min. The culture medium was then replaced with prewarmed (37°C) medium without nocodazole to allow MT regrowth. After MT regrowth for 0, 30, 60, and 120 s, the cells were washed with PBS and fixed with cold methanol at –20°C. The coverslips were subsequently processed for immunofluorescence staining and confocal imaging. For live cell time-lapse imaging, cells were grown on 35-mm coverslips and treated with 100 ng/ml nocodazole for 4 h at 37°C. The cells were placed in an environmental chamber, and MT regrowth was observed using confocal microscopy at 37°C after nocodazole wash out with 37°C medium.

Immunofluorescence staining and confocal microscopy

For immunofluorescence staining, cells were washed with PBS followed by fixation with either 4% paraformaldehyde in PBS for 15 min (followed by permeabilization with 0.2% Triton X-100 in PBS for 5 min) or cold methanol (for centrosome visualization) for 10 min at –20°C. After blocking with 2% bovine serum albumin (BSA) in PBS for 30 min. The cells were then incubated with primary antibodies in PBS with 1% BSA for 2 h. Cells were washed three times with PBS (10 min each time) and incubated with a secondary antibody in PBS with 1% BSA for 1 h. After three additional washes with PBS, the coverslips were mounted on slides with mounting medium (Mowiol 4-88, Carl Roth). For confocal microscopy, the samples were imaged using a Carl Zeiss LSM880 Airyscan system with a 63× /1.4 NA or 100× /1.4 NA oil objective lenses and 405-, 488-, or 543-nm lasers.

Time-lapse microscopy

COS-7 cells stably expressed low levels of EB1-GFP and EMTB-mCherry. Cells seeded on 35-mm glass coverslips were used to acquire time-lapse images on a ZEISS spinning disk microscope with a 63x/1.4 oil Plan-Apochromat DIC objective (ZEISS Cell Observer SD Spinning Disk Confocal Microscope). MT regrowth (nucleation rates) was determined by measuring the number of MTs (EMTB-mCherry) that grew from the centrosomes and is presented as the average numbers of MTs nucleated per minute. The time-lapse images used to measure MT nucleation rates were acquired at 5-s intervals at an exposure time of 50–200 ms. Time-lapse images for measurement of EB1 comet states from the centrosome were acquired at 5-s (final time 120 s) intervals at an exposure time of 200 ms. We drew a circle of radius 1 µm around the centromere and measured the number of EB1 comets emanating from the centrosome within this circle using Imaris Lineage/Track. Time-lapse images for analysis of EB1 comet growth speed were acquired at 1-s intervals (final time 120 s) and an exposure time of 200 ms. An automated tracking program (Imaris Lineage/Track) was used to track EB1 comets and to calculate their rate of movement.

Image analysis

The image sets used to quantify the fluorescence intensities in the control and experimental groups were acquired under identical conditions. To measure Arl4D fluorescence intensity at the centrosome, we used γ-tubulin dots to generate a circle centered around the centrosome (inner area) and quantified the fluorescence intensity of Arl4D in the inner area. We also defined a second, concentric circle with a radius twice that of the inner area; the region inside this circle but outside the inner area was defined as the outer area, and we quantified the fluorescence intensity of Arl4D in the outer area. The mean Arl4D signal in the outer area was used to determine the local background fluorescence intensity, and the background intensity was subtracted from each image prior to quantification (adjusted intensity = mean fluorescence intensity of inner area – mean fluorescence intensity of outer area). For quantitation of centrosomal MTs, images were acquired as 3D confocal z-stacks. Images from the stacks were flattened by maximum intensity projection. The centrosomal MTs were then counted manually. All image processing and quantification steps were performed using ImageJ software.

Statistical analysis

Statistical comparisons between treatments were performed using the nonparametric *t* test (Student's *t* test) or one-way analysis of variance (ANOVA) in GraphPad Prism. Statistically significant differences are indicated in the figures ($*P < 0.05$, $**P < 0.01$, $***P < 0.001$, $****P < 0.0001$).

ACKNOWLEDGMENTS

We thank Joel Moss, Randy Haun, Chia-Jung Yu, and Ya-Wen Liu for their critical review of this paper. We also thank the Transgenic Mouse Models Core Facility of the College of Medicine at National Taiwan University for providing MEFs from Arl4D$^{-/-}$ mice. Finally, we thank the Image Core of the College of Medicine at National Taiwan University for providing confocal microscopy and image analyses. This work was supported by grants from the National Health Research Institutes (NHRI) of Taiwan (NHRI-EX106-10601B1) and the

Center of Precision Medicine from the Featured Areas Research Center Program within the framework of the Higher Education Sprout Project of the Ministry of Education in Taiwan awarded to F.-J.S.L.

REFERENCES

Akhmanova A, Steinmetz MO (2010). Microtubule +TIPs at a glance. J Cell Sci 123, 3415–3419.

Askham JM, Vaughan KT, Goodson HV, Morrison EE (2002). Evidence that an interaction between EB1 and p150(Glued) is required for the formation and maintenance of a radial microtubule array anchored at the centrosome. Mol Biol Cell 13, 3627–3645.

Auth T, Kunkel E, Grummt F (2006). Interaction between HP1alpha and replication proteins in mammalian cells. Exp Cell Res 312, 3349–3359.

Barral DC, Seabra MC (2004). The melanosome as a model to study organelle motility in mammals. Pigment Cell Res 17, 111–118.

Bouissou A, Vérollet C, de Forges H, Haren L, Bellaïche Y, Perez F, Merdes A, Raynaud-Messina B (2014). γ-Tubulin ring complexes and EB1 play antagonistic roles in microtubule dynamics and spindle positioning. EMBO J 33, 114–128.

Bu W, Su LK (2003). Characterization of functional domains of human EB1 family proteins. J Biol Chem 278, 49721–49731.

Chen KJ, Chiang TC, Yu CJ, Lee FS (2020). Cooperative recruitment of Arl4A and Pak1 to the plasma membrane contributes to sustained Pak1 activation for cell migration. J Cell Sci 133.

Chiang TS, Wu HF, Lee FS (2017). ADP-ribosylation factor-like 4C binding to filamin-A modulates filopodium formation and cell migration. Mol Biol Cell 28, 3013–3028.

Coquelle FM, Vitre B, Arnal I (2009). Structural basis of EB1 effects on microtubule dynamics. Biochem Soc Trans 37, 997–1001.

D'Souza-Schorey C, Chavrier P (2006). ARF proteins: roles in membrane traffic and beyond. Nat Rev Mol Cell Biol 7, 347–358.

Delgehyr N, Sillibourne J, Bornens M (2005). Microtubule nucleation and anchoring at the centrosome are independent processes linked by ninein function. J Cell Sci 118, 1565–1575.

Donaldson JG, Jackson CL (2011). ARF family G proteins and their regulators: roles in membrane transport, development and disease. Nat Rev Mol Cell Biol 12, 362–375.

Efimov A, Kharitonov A, Efimova N, Loncarek J, Miller PM, Andreyeva N, Gleeson P, Galjart N, Maia AR, McLeod IX, *et al.*, (2007). Asymmetric CLASP-dependent nucleation of noncentrosomal microtubules at the trans-Golgi network. Dev Cell 12, 917–930.

Hayashi I, Wilde A, Mal TK, Ikura M (2005). Structural basis for the activation of microtubule assembly by the EB1 and p150Glued complex. Mol Cell 19, 449–460.

Honnappa S, Gouveia SM, Weisbrich A, Damberger FF, Bhavesh NS, Jawhari H, Grigoriev I, van Rijssel FJ, Buey RM, Lawera A, *et al.*, (2009). An EB1-binding motif acts as a microtubule tip localization signal. Cell 138, 366–376.

Honnappa S, John CM, Kostrewa D, Winkler FK, Steinmetz MO (2005). Structural insights into the EB1-APC interaction. EMBO J 24, 261–269.

Jacobs S, Schilf C, Fliegert F, Koling S, Weber Y, Schurmann A, Joost HG (1999). ADP-ribosylation factor (ARF)-like 4, 6, and 7 represent a subgroup of the ARF family characterization by rapid nucleotide exchange and a nuclear localization signal. FEBS Lett 456, 384–388.

Jin H, White SR, Shida T, Schulz S, Aguiar M, Gygi SP, Bazan JF, Nachury MV (2010). The conserved Bardet-Biedl syndrome proteins assemble a coat that traffics membrane proteins to cilia. Cell 141, 1208–1219.

Juwana JP, Henderikx P, Mischo A, Wadle A, Fadle N, Gerlach K, Arends JW, Hoogenboom H, Pfreundschuh M, Renner C (1999). EB/RP gene family encodes tubulin binding proteins. Int J Cancer 81, 275–284.

Li CC, Chiang TC, Wu TS, Pacheco-Rodriguez G, Moss J, Lee FJ (2007). ARL4D recruits cytohesin-2/ARNO to modulate actin remodeling. Mol Biol Cell 18, 4420–4437.

Li CC, Wu TS, Huang CF, Jang LT, Liu YT, You ST, Liou GG, Lee FJ (2012). GTP-binding-defective ARL4D alters mitochondrial morphology and membrane potential. PLoS One 7, e43552.

Lin YC, Chiang TC, Liu YT, Tsai YT, Jang LT, Lee FJ (2011). ARL4A acts with GCC185 to modulate Golgi complex organization. J Cell Sci 124, 4014–4026.

Lin CY, Huang PH, Liao WL, Cheng HJ, Huang CF, Kuo JC, Patton WA, Massenburg D, Moss J, Lee FJ (2000). ARL4, an ARF-like protein that is developmentally regulated and localized to nuclei and nucleoli. J Biol Chem 275, 37815–37823.

Lin CY, Li CC, Huang PH, Lee FJ (2002). A developmentally regulated ARF-like 5 protein (ARL5), localized to nuclei and nucleoli, interacts with heterochromatin protein 1. J Cell Sci 115, 4433–4445.

Louie RK, Bahmanyar S, Siemers KA, Votin V, Chang P, Stearns T, Nelson WJ, Barth AI (2004). Adenomatous polyposis coli and EB1 localize in close proximity of the mother centriole and EB1 is a functional component of centrosomes. J Cell Sci 117, 1117–1128.

Nakagawa H, Koyama K, Murata Y, Morito M, Akiyama T, Nakamura Y (2000). EB3, a novel member of the EB1 family preferentially expressed in the central nervous system, binds to a CNS-specific APC homologue. Oncogene 19, 210–216.

Nakamura M, Zhou XZ, Lu KP (2001). Critical role for the EB1 and APC interaction in the regulation of microtubule polymerization. Curr Biol 11, 1062–1067.

Pasqualato S, Renault L, Cherfils J (2002). Arf, Arl, Arp and Sar proteins: a family of GTP-binding proteins with a structural device for 'front-back' communication. EMBO Rep 3, 1035–1041.

Renner C, Pfitzenmeier JP, Gerlach K, Held G, Ohnesorge S, Sahin U, Bauer S, Pfreundschuh M (1997). RP1, a new member of the adenomatous polyposis coli-binding EB1-like gene family, is differentially expressed in activated T cells. J Immunol 159, 1276–1283.

Schrøder JM, Schneider L, Christensen ST, Pedersen LB (2007). EB1 is required for primary cilia assembly in fibroblasts. Curr Biol 17, 1134–1139.

Slep KC, Rogers SL, Elliott SL, Ohkura H, Kolodziej PA, Vale RD (2005). Structural determinants for EB1-mediated recruitment of APC and spectraplakins to the microtubule plus end. J Cell Biol 168, 587–598.

Strickland LI, Wen Y, Gundersen GG, Burgess DR (2005). Interaction between EB1 and p150glued is required for anaphase astral microtubule elongation and stimulation of cytokinesis. Curr Biol 15, 2249–2255.

Su LK, Burrell M, Hill DE, Gyuris J, Brent R, Wiltshire R, Trent J, Vogelstein B, Kinzler KW (1995). APC binds to the novel protein EB1. Cancer Res 55, 2972–2977.

Su LK, Qi Y (2001). Characterization of human MAPRE genes and their proteins. Genomics 71, 142–149.

Sztul E, Chen PW, Casanova JE, Cherfils J, Dacks JB, Lambright DG, Lee FS, Randazzo PA, Santy LC, Schürmann A, *et al.*, (2019). ARF GTPases and their GEFs and GAPs: concepts and challenges. Mol Biol Cell 30, 1249–1271.

Vaughan KT (2005). TIP maker and TIP marker; EB1 as a master controller of microtubule plus ends. J Cell Biol 171, 197–200.

Wen Y, Eng CH, Schmoranzer J, Cabrera-Poch N, Morris EJ, Chen M, Wallar BJ, Alberts AS, Gundersen GG (2004). EB1 and APC bind to mDia to stabilize microtubules downstream of Rho and promote cell migration. Nat Cell Biol 6, 820–830.

Wiens CJ, Tong Y, Esmail MA, Oh E, Gerdes JM, Wang J, Tempel W, Rattner JB, Katsanis N, Park HW, *et al.*, (2010). Bardet-Biedl syndrome-associated small GTPase ARL6 (BBS3) functions at or near the ciliary gate and modulates Wnt signaling. J Biol Chem 285, 16218–16230.

Wu J, Akhmanova A (2017). Microtubule-organizing centers. Annu Rev Cell Dev Biol 33, 51–75.

Yamauchi J, Miyamoto Y, Torii T, Mizutani R, Nakamura K, Sanbe A, Koide H, Kusakawa S, Tanoue A (2009). Valproic acid-inducible Arl4D and cytohesin-2/ARNO, acting through the downstream Arf6, regulate neurite outgrowth in N1E-115 cells. Exp Cell Res 315, 2043–2052.

Zanic M, Widlund PO, Hyman AA, Howard J (2013). Synergy between XMAP215 and EB1 increases microtubule growth rates to physiological levels. Nat Cell Biol 15, 688–693.

Zhou C, Cunningham L, Marcus AI, Li Y, Kahn RA (2006). Arl2 and Arl3 regulate different microtubule-dependent processes. Mol Biol Cell 17:2476–2487.